



Cancer Research

VEGF and c-Met Blockade Amplify Angiogenesis Inhibition in Pancreatic Islet Cancer

Weon-Kyoo You, Barbara Sennino, Casey W. Williamson, et al.

Cancer Res 2011;71:4758-4768. Published OnlineFirst May 25, 2011.

Updated version Access the most recent version of this article at:
doi:[10.1158/0008-5472.CAN-10-2527](https://doi.org/10.1158/0008-5472.CAN-10-2527)

Supplementary Material Access the most recent supplemental material at:
<http://cancerres.aacrjournals.org/content/suppl/2011/05/25/0008-5472.CAN-10-2527.DC1.html>

Cited Articles This article cites by 48 articles, 17 of which you can access for free at:
<http://cancerres.aacrjournals.org/content/71/14/4758.full.html#ref-list-1>

Citing articles This article has been cited by 10 HighWire-hosted articles. Access the articles at:
<http://cancerres.aacrjournals.org/content/71/14/4758.full.html#related-urls>

E-mail alerts [Sign up to receive free email-alerts](#) related to this article or journal.

Reprints and Subscriptions To order reprints of this article or to subscribe to the journal, contact the AACR Publications Department at
pubs@aacr.org.

Permissions To request permission to re-use all or part of this article, contact the AACR Publications Department at
permissions@aacr.org.

VEGF and c-Met Blockade Amplify Angiogenesis Inhibition in Pancreatic Islet Cancer

Weon-Kyoo You¹, Barbara Sennino¹, Casey W. Williamson¹, Beverly Falcón¹, Hiroya Hashizume¹, Li-Chin Yao¹, Dana T. Aftab², and Donald M. McDonald¹

Abstract

Angiogenesis inhibitors that block VEGF receptor (VEGFR) signaling slow the growth of many types of tumors, but eventually the disease progresses. Multiple strategies are being explored to improve efficacy by concurrent inhibition of other functionally relevant receptor tyrosine kinases (RTK). XL880 (foretinib, GSK1363089) and XL184 (cabozantinib) are small-molecule inhibitors that potently block multiple RTKs, including VEGFR and the receptor of hepatocyte growth factor c-Met, which can drive tumor invasion and metastasis. This study compared the cellular effects of XL880 and XL184 with those of an RTK inhibitor (XL999) that blocks VEGFR but not c-Met. Treatment of RIP-Tag2 mice with XL999 resulted in 43% reduction in vascularity of spontaneous pancreatic islet tumors over 7 days, but treatment with XL880 or XL184 eliminated approximately 80% of the tumor vasculature, reduced pericytes and empty basement membrane sleeves, caused widespread intratumoral hypoxia and tumor cell apoptosis, and slowed regrowth of the tumor vasculature after drug withdrawal. Importantly, XL880 and XL184 also decreased invasiveness of primary tumors and reduced metastasis. Overall, these findings indicate that inhibition of c-Met and functionally related kinases amplifies the effects of VEGFR blockade and leads to rapid, robust, and progressive regression of tumor vasculature, increased intratumoral hypoxia and apoptosis, and reduced tumor invasiveness and metastasis. *Cancer Res*; 71(14); 4758–68. ©2011 AACR.

Introduction

Inhibitors of VEGF signaling block VEGF-driven angiogenesis, prune VEGF-dependent blood vessels, and normalize vessels that do not regress (1–4). VEGF inhibitors can also promote tumor invasion and metastasis in some preclinical models (5, 6), but the underlying mechanism is still unclear (7, 8). Treatment of cancer patients with VEGF inhibitors can slow tumor growth and in some cases prolong survival, but resistance eventually develops and the disease progresses through growth of residual primary tumor or metastases (9–12). Inhibitors that target other pathways, such as those involved in tumor invasiveness, are therefore being developed (13, 14).

Hepatocyte growth factor (HGF, scatter factor), through its HGF receptor (HGFR) c-Met, is a potent motility factor and mitogen (15–18). HGF and c-Met are upregulated in many

human cancers and contribute to tumor growth, angiogenesis, invasiveness, and metastasis (19, 20). Inhibition of the HGF/c-Met pathway can reduce tumor growth, angiogenesis, and metastasis in preclinical models (21–24).

c-Met expression is increased by hypoxia through activation of hypoxia inducible factor-1α (HIF-1α) and contributes to the aggressiveness of hypoxic tumors (25). HIF-1α-induced c-Met expression could be triggered by vascular pruning caused by VEGF inhibitors and could select for migratory, invasive tumor cells and predispose spread by metastasis (26). The strategic roles of VEGF receptor (VEGFR) and c-Met signaling in tumor angiogenesis, invasion, and metastasis make these receptors attractive therapeutic targets (16–18, 27).

We examined the effects of 2 small-molecule receptor tyrosine kinase (RTK) inhibitors, XL880 (foretinib, GSK1363089) and XL184 (cabozantinib), that block phosphorylation of c-Met and VEGFR at nanomolar or subnanomolar concentrations (27–29) to assess the interaction of these receptors in tumors. As set out in Table 1, both XL880 and XL184 block c-Met and VEGFR-2. In addition, XL880 inhibits AXL, Tie2, KIT, FLT3, platelet-derived growth factor receptor (PDGFR), and RON (27, 30, 31), and XL184 inhibits AXL, Tie2, KIT, FLT3, and RET but not PDGFR or RON (28, 29, 32). The lack of overlap of PDGFR and RON makes these receptors unlikely to explain the mutual effects of XL880 and XL184 on tumors.

The effects of a third RTK inhibitor, XL999, which blocks VEGFR, PDGFR, fibroblast growth factor receptor (FGFR), FLT3, KIT, and AXL, was used for comparison because it

Authors' Affiliations: ¹Cardiovascular Research Institute, Comprehensive Cancer Center, and Department of Anatomy, University of California, San Francisco; and ²Exelixis Inc., South San Francisco, California

Note: Supplementary data for this article are available at *Cancer Research* Online (<http://cancerres.aacrjournals.org>).

Corresponding Author: Donald M. McDonald, Department of Anatomy, University of California, 513 Parnassus Avenue, Room S1363, San Francisco, CA 94143. Phone: 415-476-2118; Fax: 415-476-4845; E-mail: donald.mcdonald@ucsf.edu

doi: 10.1158/0008-5472.CAN-10-2527

©2011 American Association for Cancer Research.

Table 1. IC₅₀ (nmol/L) values of XL880, XL184, XL999, and sorafenib on kinase activity

Kinases	VEGFR-2 (KDR)	c-MET (HGFR)	FGFR1	PDGFR- β	KIT	FLT1	FLT4	FLT3	Tie2	AXL	RON
XL880 (27, 31)	0.86	0.4	660	9.6	6.7	6.8	2.8	3.6	1.1	11	3
XL184 (29, 32)	0.035	1.3	5,294	234	4.6	12	6.0	11.3	14.3	7.0	124
XL999 (33, 34)	2.6	463		8.2	1.5	13.8	29	3.0	0.8	270	4.6
Sorafenib (50)	90	–	580	57	68	–	–	33	–	–	–

NOTE: IC₅₀ values (nmol/L) for inhibition of phosphorylation of 11 receptor tyrosine kinases by XL880, XL184, and XL999 show similarities for VEGFR-2, KIT, and AXL and differences for c-MET. XL880 and XL184 differ in inhibition of PDGFR- β and RON, and neither inhibits FGFR1. IC₅₀ values of sorafenib are shown for comparison.

does not block c-Met but does block many other targets of XL880 and XL184 (33, 34). Spontaneous pancreatic islet tumors in RIP-Tag2 transgenic mice were used as a model (4, 35, 36), and the abundance, cellular composition, and receptor expression of tumor blood vessels, intratumoral hypoxia, and measures of tumor aggressiveness were used as readouts.

Our studies revealed that XL880 or XL184, but not XL999, led to rapid, widespread, and progressive regression of tumor vasculature, extensive hypoxia, and apoptosis of tumor cells and decreased tumor aggressiveness.

Materials and Methods

Animals

RIP-Tag2 mice in a C57BL/6 background were used as the tumor model (35). All experiments were approved by the University of California, San Francisco, Institutional Animal Care and Use Committee.

Treatments

RIP-Tag2 mice were 10-week-olds at the onset of treatment, unless otherwise indicated. XL880 (foretinib, GSK1363089), XL184 (cabozantinib), and XL999 were suspended at a concentration of 5 mg/mL in sterile saline or water and administered by gavage, daily for 7 days (see Supplementary Materials and Methods).

Detection of functional blood vessels and hypoxia

Functional blood vessels in tumors were identified and marked by fluorescein isothiocyanate (FITC)-labeled *Lycopersicon esculentum* lectin (LEA; 1 mg/mL, 100 μ L; Vector Laboratories), injected via a tail vein (i.v.) 2 minutes before the perfusion of fixative (4). Hypoxic regions of tumors were identified by pimonidazole hydrochloride (60 mg/kg, 2.5 μ L/g of mouse body weight; Hypoxyprobe Plus Kit HP2; Chemicon) injected i.v. 1 hour before the perfusion (5).

Tissue fixation and immunohistochemistry

Mice were perfused through the heart with paraformaldehyde fixative (4, 36). Cryostat sections (80 μ m in thickness) were stained with combinations of the antibodies (see Supplementary Materials and Methods).

Imaging and analysis

Specimens were examined with a Zeiss Axiohot fluorescence microscope and a Zeiss LSM 510 laser scanning confocal microscope. Area densities of endothelial cells, pericytes, basement membrane, apoptotic cells, and hypoxic regions were calculated from digital fluorescence microscopic images, using an empirically determined threshold value of 30 to 50 (4, 36). Intensity of VEGFR-2, VEGFR-3, and E-cadherin immunofluorescence was measured (4, 36). Metastases of RIP-Tag2 tumors were identified in sections of liver stained for SV40 T-antigen. Vascularity of the trachea was expressed as the average number of capillaries that crossed cartilage rings (10 rings/mouse, 4–5 mice/group; ref. 37).

Tumor size and Invasion index

The size of tumors in the pancreas from RIP-Tag2 mice treated with vehicle, XL880, or XL184 for 7 days (5 mice/group) was assessed in 80- μ m sections stained for insulin or SV40 T-antigen and expressed as the sectional area of tumor (4).

Invasion index was measured using ImageJ on fluorescence microscopic images (5 \times objective, 1 \times Optovar) of 80- μ m sections of pancreas stained for insulin or SV40 T-antigen (red) and amylase (green channel). The red channel of RGB images was converted to 8-bit gray scale, and the tumor border was outlined using the freehand tool. Regions outside the tumor were filled black. A threshold in the range of 0 to 255 was applied to include all tumor cells and then the image was converted to binary. Invasion index (values \geq 1.0) was calculated from the area and perimeter of the tumor by the formula: $1/(4\pi \times \text{area}/\text{perimeter}^2)$, where a circle has a value of 1.0. The median Invasion index was calculated for all tumors in each mouse (10–21 tumors/mouse). The mean Invasion index for each group was calculated from the median value for each mouse (4 mice/group).

Immunoprecipitation and quantitative reverse transcriptase-PCR

Immunoprecipitation and quantitative reverse transcriptase-PCR analysis were carried out as described in Supplementary Materials and Methods.

Statistics

Values are expressed as means \pm SE (4–6 mice/group). The significance of differences between groups was assessed by

ANOVA, followed by the Bonferroni–Dunn or Fisher test for multiple comparisons ($P < 0.05$ values were considered significant).

Results

Massive regression of tumor vessels after XL880 or XL184 treatment

Blood vessels in RIP-Tag2 tumors were abundant, irregular, and tortuous under baseline conditions [Fig. 1A (i)] but were sparse after XL880 treatment for 7 days [Fig. 1A (ii)]. Loss of tumor vessels was dose and time dependent. Reductions ranged from 40% at 10 mg/kg to 80% at 60 mg/kg [Fig. 1A (iii)]. Time course studies revealed no reduction at 6 hours, 40% reduction at 1 day, 76% at 7 days, and 90% at 14 days [Fig. 1B (i–iv)]. Tumor vascularity decreased after XL184

treatment [Fig. 1C (i and ii)], with reductions ranging from 67% at 3 mg/kg to 83% at 30 mg/kg for 7 days [Fig. 1C (iii)].

XL999, which inhibits VEGFR but not c-Met, reduced the vascularity of RIP-Tag2 tumors, but the magnitude of the reduction at 7 days (43%) was significantly less than after XL880 (80%) or XL184 (77%) treatment [Fig. 1D (i)], and the surviving blood vessels were different. After XL880 or XL184 treatment for 7 days or longer, many remaining tumor vessels were narrow, variable in diameter, and appeared fragmented [Fig. 1D (ii)]. In contrast, most tumor vessels present after XL999 treatment for 7 days were larger, more uniform in caliber ("normalized"), and had less branching and fewer sprouts than present under baseline conditions [Fig. 1D (iii)].

Because of evidence that some capillaries of normal organs regress after VEGF inhibition (4, 38, 39), we investigated this

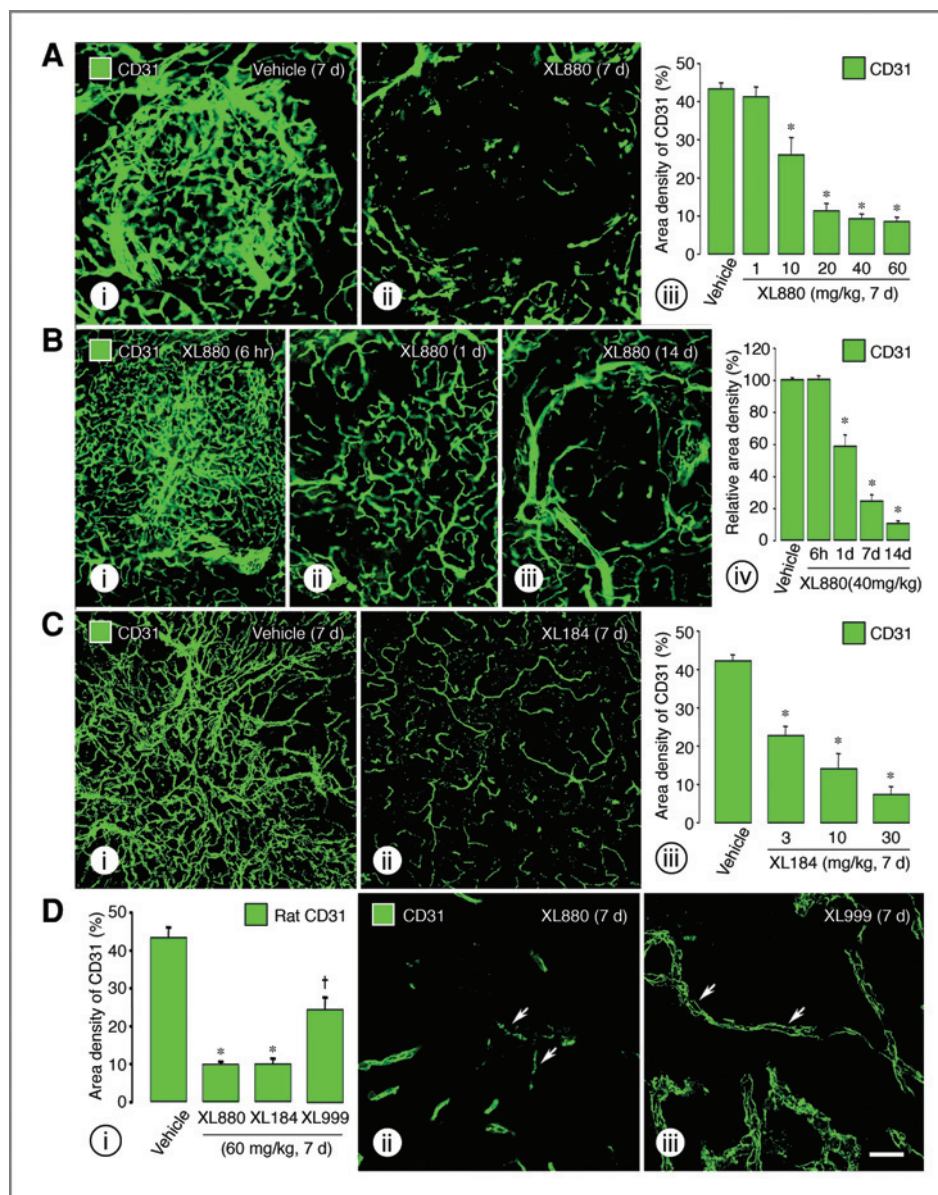


Figure 1. Effects of XL880, XL184, and XL999 on tumor vessels. Fluorescence micrographs compare the vasculature of RIP-Tag2 tumors stained for CD31 immunoreactivity. A, i and ii, vascularity is conspicuously greater after vehicle than after XL880 treatment (60 mg/kg) for 7 days. A, iii, dose-response of tumor vessel regression after XL880 treatment for 7 days. B, i–iii, no reduction of vascularity at 6 hours after XL880 treatment (40 mg/kg) but conspicuous reductions after 1 day or 14 days. B, iv, time course of reduction in tumor vascularity after XL880 treatment. C, i and ii, reduction in vascularity after XL184 treatment (30 mg/kg) for 7 days. C, iii, dose-response after XL184 treatment for 7 days. D, i, smaller reduction in vascularity after XL999 than after XL880 or XL184 treatment. D, ii, narrow, irregular, or fragmented tumor vessels (arrows) still present after XL880 or XL184 treatment for 7 days. D, iii, larger and less tortuous tumor vessels (arrows) remain after XL999 treatment for 7 days. *, $P < 0.001$ versus vehicle. †, $P < 0.001$ versus XL880 and XL184. Scale bar, 120 μ m (A–C); 30 μ m (D).

effect of XL880 and found consistent reductions in the number of capillaries in the trachea, thyroid, choriocapillaris of the eye, and jejunum (Supplementary Fig. S1).

Reduction in VEGFR-2 and VEGFR-3

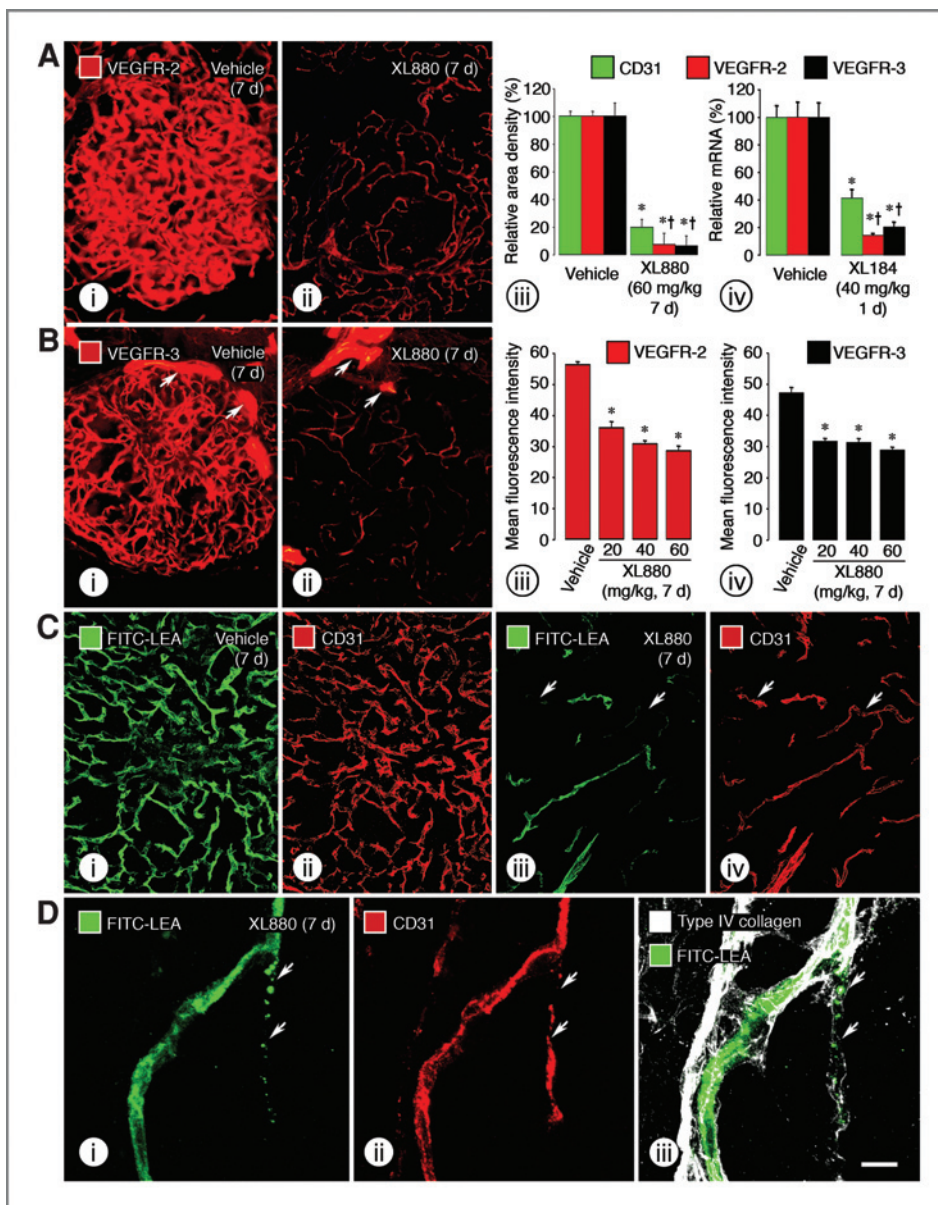
Strong and widespread VEGFR-2 immunoreactivity highlighted the dense vascularity of RIP-Tag2 tumors under baseline conditions [Fig. 2A (i)] but was conspicuously reduced after XL880 treatment [Fig. 2A (ii)]. Overall, VEGFR-2 immunoreactivity was reduced by 93% after the 7-day treatment [Fig. 2A (iii)]. The speed of the change was evident by the 86% reduction in the expression of VEGFR-2 mRNA after only 1 day [Fig. 2A (iv)].

VEGFR-3 immunoreactivity was also strong and widespread on tumor vessels and was sharply reduced by XL880 treatment for 7 days [Fig. 2B (i and ii)]. Overall, VEGFR-3

immunoreactivity was reduced by 94% at 7 days [Fig. 2A (iii)], which was obvious in blood vessels but did not occur in peritumoral lymphatics [Fig. 2B (ii), arrows]. Expression of VEGFR-3 mRNA was reduced by 80% after 1 day only [Fig. 2A (iv)].

The large reductions in VEGFR-2 and VEGFR-3 immunoreactivity in treated tumors [Fig. 2A (iii)] resulted from 2 changes: (i) decreased vascularity, reflected by the reduction in number of tumor vessels [Fig. 2A (ii) and B (ii)], and (ii) decreased receptor protein in the surviving tumor vessels, reflected by the dose-dependent decrease in brightness of immunofluorescence [Fig. 2B (iii and iv)]. Because of this dual effect, the reductions in overall VEGFR-2 and VEGFR-3 immunoreactivity and expression were significantly greater than the corresponding reductions in CD31 [Fig. 2A (iii and iv)].

Figure 2. VEGFR-2 and VEGFR-3 expression and vessel function. Confocal micrographs of RIP-Tag2 tumors. A, i, strong VEGFR-2 immunoreactivity after vehicle. A, ii, weak VEGFR-2 after XL880 treatment for 7 days. A, iii, reductions in CD31, VEGFR-2, and VEGFR-3 immunoreactivities after XL880 treatment (60 mg/kg, 7 days). A, iv, significantly reduced expression of VEGFR-2 and VEGFR-3 mRNA after XL184 treatment (40 mg/kg, 1 day) compared with smaller reduction in CD31 mRNA. B, i, strong VEGFR-3 staining in tumor vessels and lymphatics (arrows) after vehicle treatment. B, ii, markedly reduced VEGFR-3 in tumor vessels but not in lymphatics (arrows) after XL880 treatment. B, iii and iv, dose-dependent reductions in fluorescence intensity of VEGFR-2 and VEGFR-3 in tumor vessels after XL880 treatment. C, i–iv, tumor vessel function assessed by i.v. injection of FITC-LEA (green) followed by staining for CD31 (red). All tumor vessels have lectin staining (uniform perfusion) after vehicle, but scattered tumor vessels lack lectin staining (nonperfused vessels, arrows) after XL880 treatment. D, i–iii, discontinuities in staining for lectin (arrows), CD31 (arrows), and basement membrane (arrows) after XL880 treatment. *, P < 0.001 versus vehicle. †, P < 0.001 versus corresponding CD31. Scale bar, 120 μm (A and B); 60 μm (C); 10 μm (D).



Impaired function of surviving tumor vessels

Blood vessel function was assessed by i.v. injection of FITC-labeled LEA, which uniformly stains the luminal surface of the endothelium of perfused blood vessels (4). Under baseline conditions, the pattern of lectin staining in tumors largely matched the distribution of CD31 staining [Fig. 2C (i and ii)], indicating that most vessels were functional. After XL880 treatment for 7 days, tumor vascularity was markedly reduced and lectin staining was absent in some of the remaining vessels [Fig. 2C (iii and iv), arrows], indicative of impaired functionality, or was discontinuous [Fig. 2D (i)] in vessels that had discontinuous staining for CD31 and type IV collagen [Fig. 2D (ii and iii)], consistent with vessels undergoing regression.

Reduction in pericytes and empty basement membrane sleeves

NG2-positive pericytes were abundant throughout RIP-Tag2 tumors under baseline conditions [Fig. 3A (i)] but were sparse after XL880 or XL184 treatment for 7 days [Fig. 3A (ii and iii)]. Measurements showed a 71% reduction in NG2 immunoreactivity after the highest dose of XL880 [Fig. 3B (i)], which was almost as large as the corresponding 80% reduction in CD31 [Fig. 1A (iii)]. The abnormally loose association of pericytes with tumor blood vessels was prominent under baseline conditions [Fig. 3B (ii)] and was still evident after XL880 treatment [Fig. 3B (iii)].

Type IV collagen immunoreactivity largely matched the CD31 staining of blood vessels in tumors at baseline

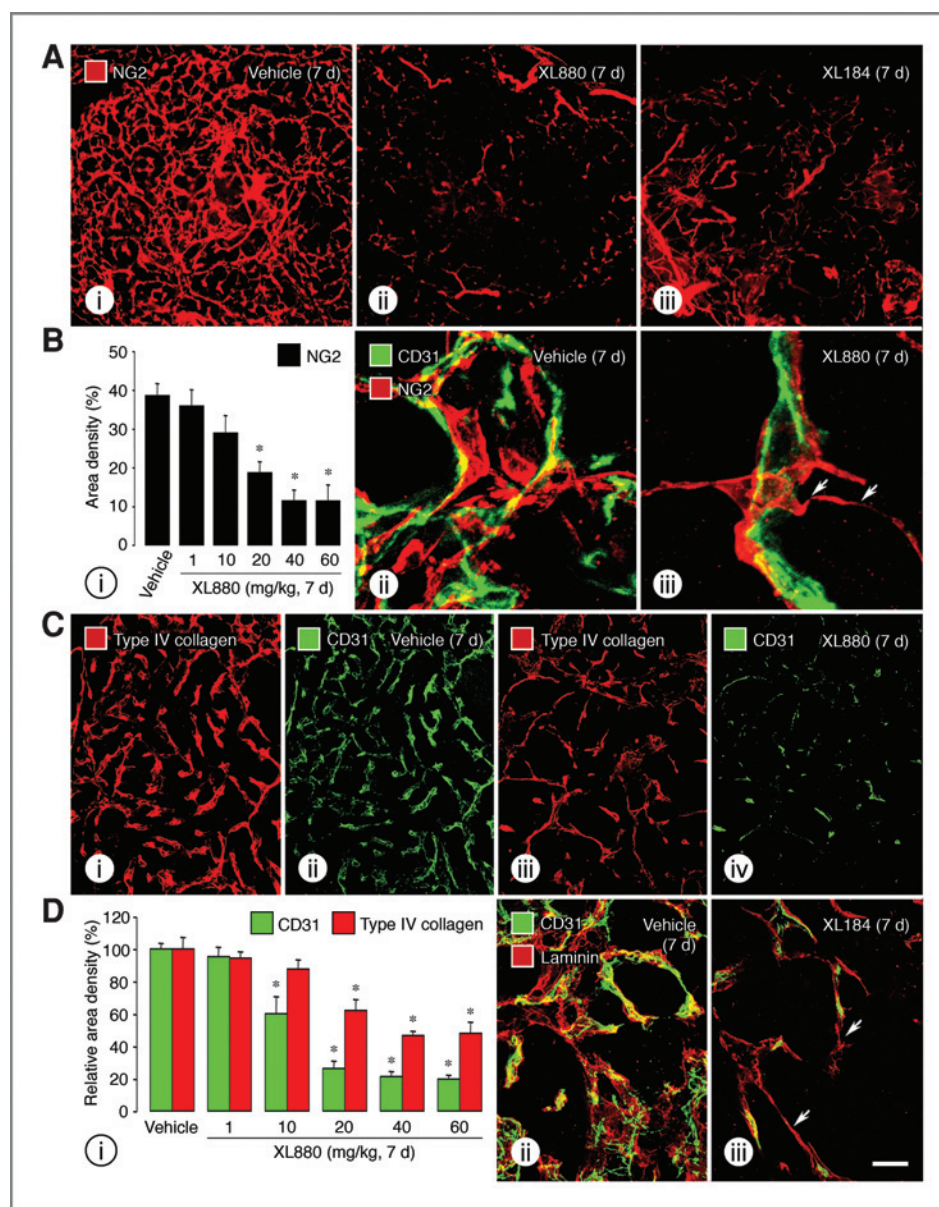


Figure 3. Reduction in pericytes and basement membrane sleeves. Confocal micrographs of RIP-Tag2 tumors. A, i, abundant NG2-positive tumor vessels after vehicle treatment, reflecting abundance of pericytes. A, ii and iii, sparse staining for NG2 after XL880 or XL184 treatment. B, i, dose-dependent NG2 reduction after XL880 treatment. B, ii and iii, loose association of NG2-positive pericytes after vehicle or XL880 treatment for 7 days (40 mg/kg, arrows). C, i–iv, type IV collagen (red) and CD31 (green) in tumors after vehicle or XL880 treatment. D, i, dose-dependent decreases in type IV collagen after XL880 treatment compared with larger reductions in CD31. Differences in amounts of type IV collagen and CD31 reflect the abundance of empty basement membrane sleeves. D, ii and iii, tumor vessels stained for laminin (red) and CD31 (green) showing more abundant empty basement membrane sleeves after XL184 treatment (arrows). Dose of XL880 or XL184, 60 mg/kg for 7 days. *, P < 0.001 versus vehicle. Scale bar, 120 μm (A); 10 μm (B); 60 μm (C); 30 μm (D).

[Fig. 3C (i and ii)]. The amount of type IV collagen was reduced after XL880 treatment for 7 days [Fig. 3C (iii)] but not as much as CD31 staining [Fig. 3C (iv)]. Measurements showed a 52% reduction in type IV collagen compared with the 80% reduction in CD31 [Fig. 3D (i)].

The number of empty basement membrane sleeves was reflected by the discrepancy between the loss of endothelial cells and the loss of basement membrane [Fig. 3D (i)]. After XL880 treatment for 7 days, about 20% of the original amount of basement membrane was on surviving tumor vessels, 28% was in the form of empty sleeves, and 52% was lost. Vascular basement membrane was similarly reduced after XL184 treatment [Fig. 3D (ii and iii)].

Regrowth of tumor vasculature

Stopping XL880 after treatment for 7 days was followed by partial regrowth of the tumor vasculature over the subsequent 7 days, but tumor vascularity did not return to the baseline [Supplementary Fig. S2A (i–iv)]. With 77% reduction in vascularity after 7-day treatment as a reference, recovery was 22% (58% below baseline) at 2 days and was 51% (29% below baseline) at 7 days [Supplementary Fig. S2B (i)]. Consistent with continuing regrowth, endothelial cell sprouts were still present at 7 days [Supplementary Fig. S2B (ii)].

Recovery of the intensity of VEGFR-2 immunofluorescence of tumor vessels was not similarly delayed. Brightness of VEGFR-2 immunofluorescence was 54% less than baseline after XL880 treatment for 7 days but was only 21% less at 2 days and was back to baseline at 7 days [Supplementary Fig. S2B (iii)]. Similarly, hypoxic regions of tumors marked by pimonidazole staining rapidly decreased after XL880 treatment was withdrawn and were not present at 7 days after treatment ended [Supplementary Fig. S2C (i–iv)].

Distribution of c-Met in tumors

Under baseline conditions, the pattern of c-Met immunoreactivity was largely vascular [Fig. 4A (i)]. About 7% of blood vessels in RIP-Tag2 tumors were stained. Vascular staining for c-Met was much less after XL880 [Fig. 4A (ii)] or XL184 [Fig. 4A (iii)] treatment but was not noticeably different after XL999 treatment for 7 days [Fig. 4A (iv)]. Colocalization with CD31 staining confirmed the association of most c-Met immunoreactivity with endothelial cells [Fig. 4B (i–iv)]. Surface plots of c-Met immunofluorescence of baseline tumors showed that the vascular pattern was surrounded by weak, uniform background fluorescence in regions where tumor cells predominated [Fig. 4C (i)]. In contrast, surface plots of tumors after XL880 or XL184 treatment lacked the vascular pattern but still had the weak background fluorescence [Fig. 4C (ii and iii)]. Neither the amount nor the distribution of c-Met immunoreactivity changed appreciably after XL999 treatment [Fig. 4C (iv)]. Colocalization of faint c-Met immunoreactivity with staining for SV40 T-antigen was consistent with weak c-Met expression in some tumor cells under baseline conditions [Fig. 4D (i)].

Pixels where c-Met immunoreactivity colocalized with CD31 decreased by at least half after XL880 or XL184 treatment, suggestive of a preferential effect on endothelial

cells [Fig. 4D (ii)]. This was not found after XL999 treatment.

Overall, c-Met protein in tumors assessed by immunoprecipitation was slightly less after XL184 treatment, but phosphorylated c-Met was markedly reduced after XL184 treatment for 7 days [Fig. 4D (iii)]. Neither of them changed after XL999 treatment [Fig. 4D (iii)].

Intratumoral hypoxia and apoptosis

Hypoxic regions marked by pimonidazole staining were sparse or absent in tumors of 10- or 11-week old RIP-Tag2 mice treated with vehicle [Fig. 5A (i)] but were abundant and conspicuous in tumors after XL880 or XL184 treatment for 7 days [Fig. 5A (ii and iii)]. Surface plots highlighted the difference between negligible pimonidazole immunofluorescence in vehicle-treated tumors and the strong, widespread staining after XL880 treatment [Fig. 5B (i)]. Pimonidazole staining was increased about 100-fold, from 11% of tumor area after XL880 treatment and 9% after XL184 treatment, compared with the baseline value of only 0.1% [Fig. 5B (ii)].

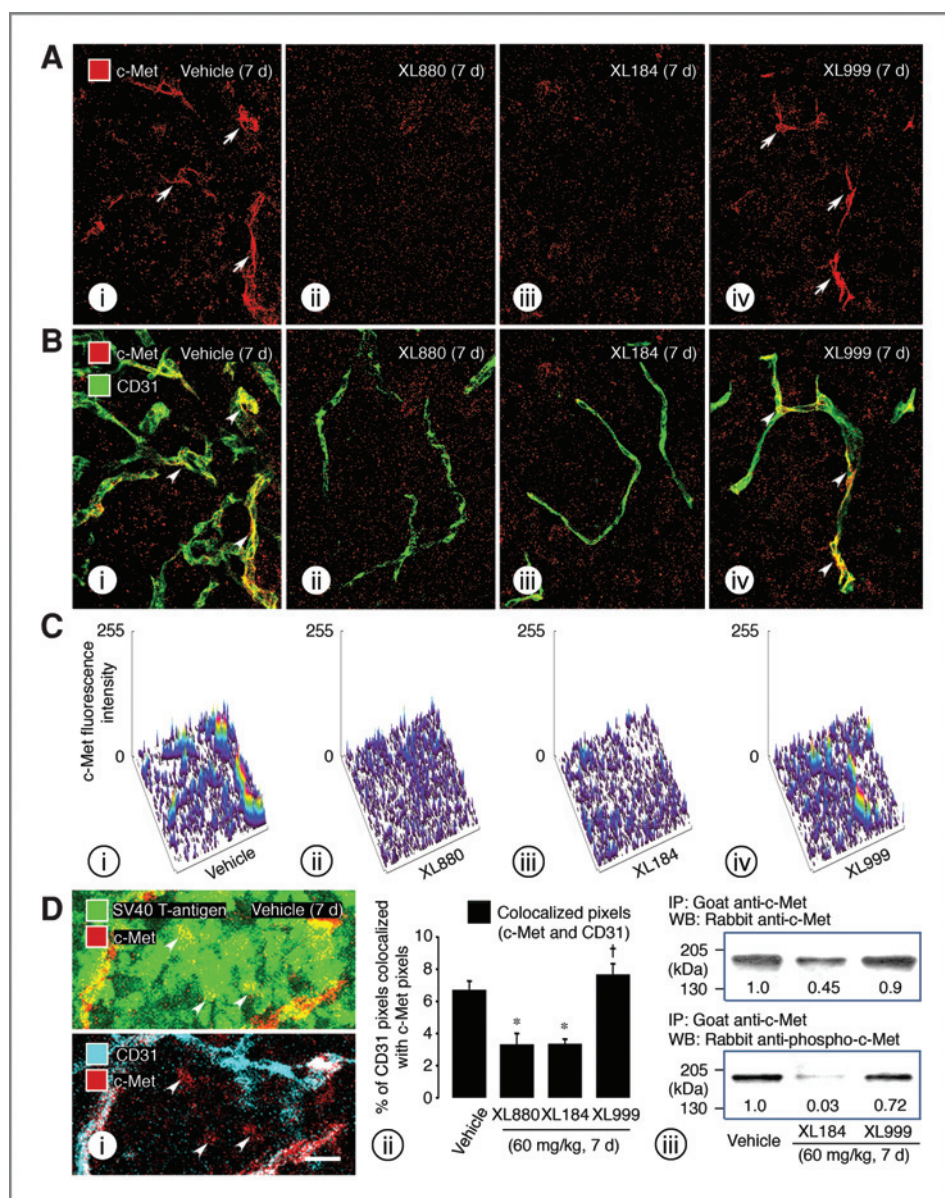
After XL880 or XL184 treatment, most pimonidazole staining was in regions of tumors that were avascular or had narrowed blood vessels [Fig. 5A (ii and iii)]. Many pimonidazole-positive regions were separated from blood vessels by sleeves of unstained tumor cells [average width $36 \pm 3 \mu\text{m}$, Fig. 5B (iii)]. Pimonidazole staining next to narrowed or fragmented tumor vessels did not have an intervening sleeve of unstained cells [Fig. 5B (iii)].

Apoptotic cells identified by activated caspase-3 immunoreactivity were scattered in baseline tumors [Fig. 5C (i)]. After XL880 or XL184 treatment, activated caspase-3 immunoreactivity was much more extensive and was associated with clumps of cells [Fig. 5C (ii)]. The fractional area of activated caspase-3 increased 5-fold after the highest dose of XL880 for 7 days [Fig. 5C (iii)]. Some activated caspase-3 immunoreactivity coincided with CD31 staining, indicative of apoptotic endothelial cells [Fig. 5D (i)]. Activated caspase-3 staining after XL184 treatment resembled that after XL880 treatment [Fig. 5C (ii) and D (ii)], but after XL999 treatment, the staining resembled that found in baseline tumors [Fig. 5C (i) and D (iii)].

Tumor aggressiveness

As indices of aggressiveness of RIP-Tag2 tumors, we examined tumor shape, E-cadherin staining, size, and metastasis to the liver. The contour of the tumor perimeter was assessed in sections stained for insulin or SV40 T-antigen in tumor cells and amylase in the surrounding acinar pancreas. Vehicle-treated tumors had irregular borders [Fig. 6A (i and ii)], but tumors treated with XL880 for 14 days had a smooth contour and distinct margin with the neighboring acinar pancreas [Fig. 6A (iii and iv)]. The irregularity of the tumor border, quantified as the Invasion index, was significantly less (value = 3.4) after XL880 treatment for 14 days than after vehicle treatment (value = 5.4; Fig. 6B (i–iii)).

E-cadherin immunoreactivity of tumor cells, as an indicator of epithelial-mesenchymal transition status (40), was faint to absent under baseline conditions [Supplementary Fig. S2D (i)]



but was stronger after XL880 or XL184 treatment for 7 days [Supplementary Fig. S2D (ii and iii)]. The mean intensity of E-cadherin immunofluorescence increased from 32 in vehicle-treated tumors to 41 after XL880 treatment and 46 after XL184 treatment for 7 days [Supplementary Fig. S2D (iv)]. The acinar pancreas and pancreatic ducts had strong E-cadherin immunoreactivity under all conditions.

Tumors in RIP-Tag2 mice treated for 7 days, beginning at age 10 weeks, were 40% smaller after XL880 treatment and 35% smaller after XL184 treatment than corresponding values for vehicle [Fig. 6C (i)].

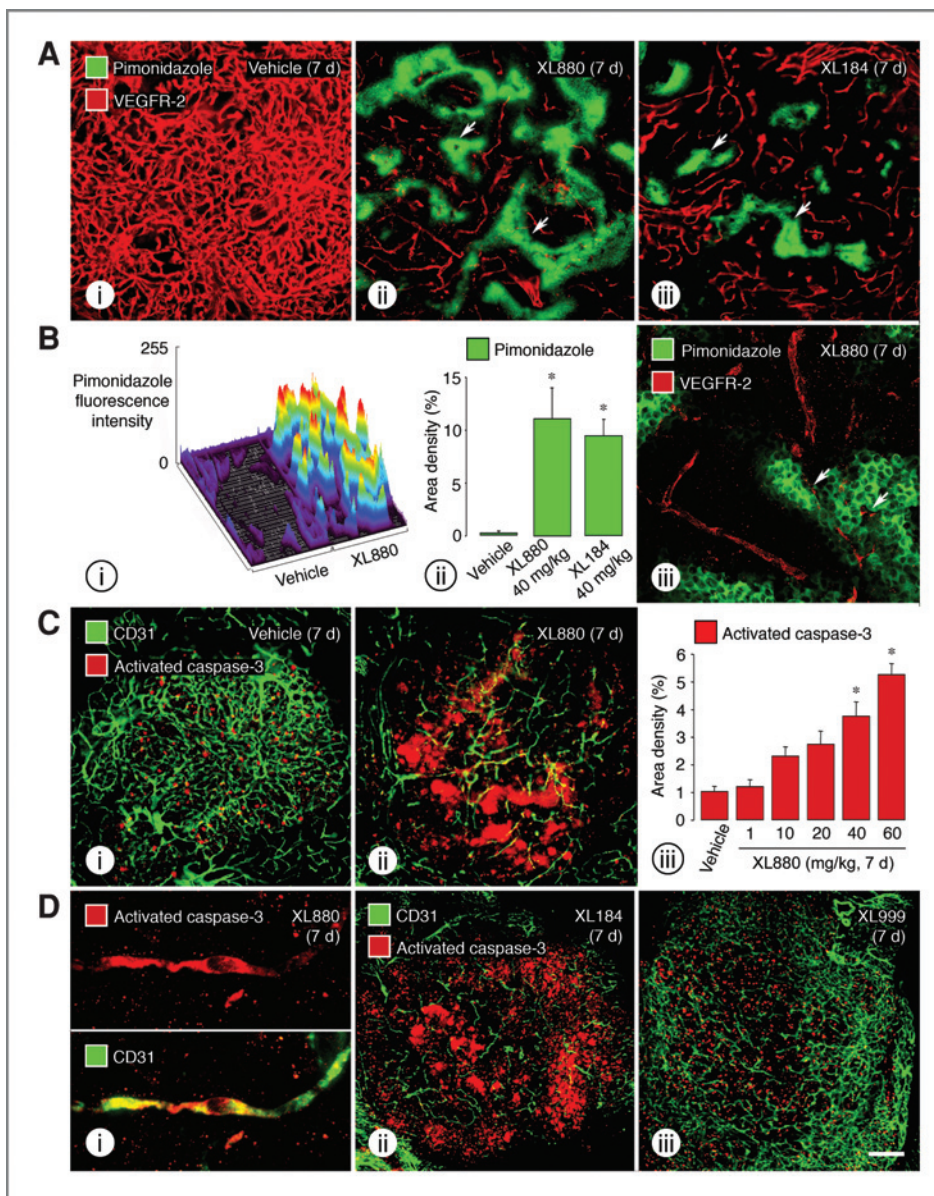
Tumor cells, identified by SV40 T-antigen immunofluorescence, were scattered in histologic sections of liver from 3 of 4 RIP-Tag2 mice treated with vehicle for 14 days [Fig. 6C (ii)], but none were found in livers of 4 mice treated with XL880 for the same period [Fig. 6C (iii)].

To determine whether RIP-Tag2 tumors become more invasive after XL880 is withdrawn, we treated mice with XL880 for 7 days, from age 10 to 11 weeks, and then studied them 7 or 14 days later. The border of tumors was irregular at baseline but was much smoother after XL880 treatment for 7 days [Fig. 6D (i and ii)]. At 7 days after treatment ended, the tumor border was still smooth, but small groups of tumor cells projected into the surrounding acinar pancreas [Fig. 6D (iii)]. At 14 days, tumors had irregular borders similar to but not greater than those at baseline [Fig. 6D (i and iv)]. Measurements of Invasion index reflected these changes [Fig. 6D (v)].

Discussion

The overall goal of this study was to determine the cellular effects of 2 small-molecule RTK inhibitors, XL880 and XL184,

Figure 5. Hypoxia and apoptosis in RIP-Tag2 tumors. A, i–iii, confocal micrographs of RIP-Tag2 tumors stained for VEGFR-2 (red, endothelial cells) and pimonidazole (green, hypoxia) show that the amount and distribution of hypoxia (arrows) increased from none after vehicle to widespread after XL880 or XL184 treatment (40 mg/kg) for 7 days. B, i, surface plot of pimonidazole fluorescence was essentially flat after vehicle treatment but had high peaks after XL880 treatment. B, ii, measurements of fractional area of pimonidazole staining in tumors. B, iii, some regions of pimonidazole staining overlapped fragmented tumor vessels (arrows) but most were separated from tumor vessels by sleeves of unstained tumor cells (dark). C, i, scattered apoptotic cells identified by activated caspase-3 staining in tumors after vehicle treatment. C, ii, widespread and clumped staining of activated caspase-3 in tumors after XL880 treatment (60 mg/kg) for 7 days. C, iii, dose-response increase of staining of activated caspase-3 in tumors after XL880 treatment for 7 days. D, i, apoptotic endothelial cells in tumor vessel stained for activated caspase-3 (top) and colocalized with CD31 (bottom) after XL880 treatment for 7 days. D, ii and iii, widespread immunoreactivity of activated caspase-3 after XL184 treatment but not after XL999 treatment (40 mg/kg) for 7 days. *, $P < 0.001$ versus vehicle. Scale bar, 120 μ m (A and C); 30 μ m (B); 10 μ m (D, i); 240 μ m (D, ii and iii).



that block key signaling pathways involved in angiogenesis and tumor invasiveness. Both inhibitors target VEGFR and c-Met at low nanomolar or subnanomolar concentrations, together with several other RTKs, and both had rapid, robust, profound, and largely similar cellular effects on blood vessels and tumor cells of RIP-Tag2 tumors. These effects differed qualitatively and quantitatively from those found after treatment with XL999, an RTK inhibitor that does not target c-Met but does block VEGFR plus multiple other receptors blocked by XL880 and XL184.

Treatment with XL880 or XL184 led to rapid and severe changes in tumor blood vessels, which were greater than after XL999 over a similar dosage range or after other VEGF inhibitors (4, 36, 41). VEGFR-2 and VEGFR-3 proteins and their respective mRNA expression were reduced even more than corresponding values for CD31, consistent with dual

effects of vessel regression and downregulation of expression on the remaining tumor vessels (4, 36).

Selective inhibition of VEGF signaling causes regression of some tumor vessels, but those that remain tend to be more normal (3, 4), which were confirmed after XL999. However, surviving tumor vessels were qualitatively different after XL880 or XL184 treatment, which were narrow, fragmented, and not stained by i.v. FITC-LEA, suggestive of continuing regression (4, 36, 41). The tumor vascularity continued to decrease during the second week of XL880 treatment. This progressive change differs from vascular regression due to many selective VEGF inhibitors, which tends to plateau after a week or so as tumor vessels normalize (3, 4).

Basement membrane sleeves and pericytes were decreased after treatment with XL880 or XL184. Some reduction was also found with XL999, as has been reported for other VEGF

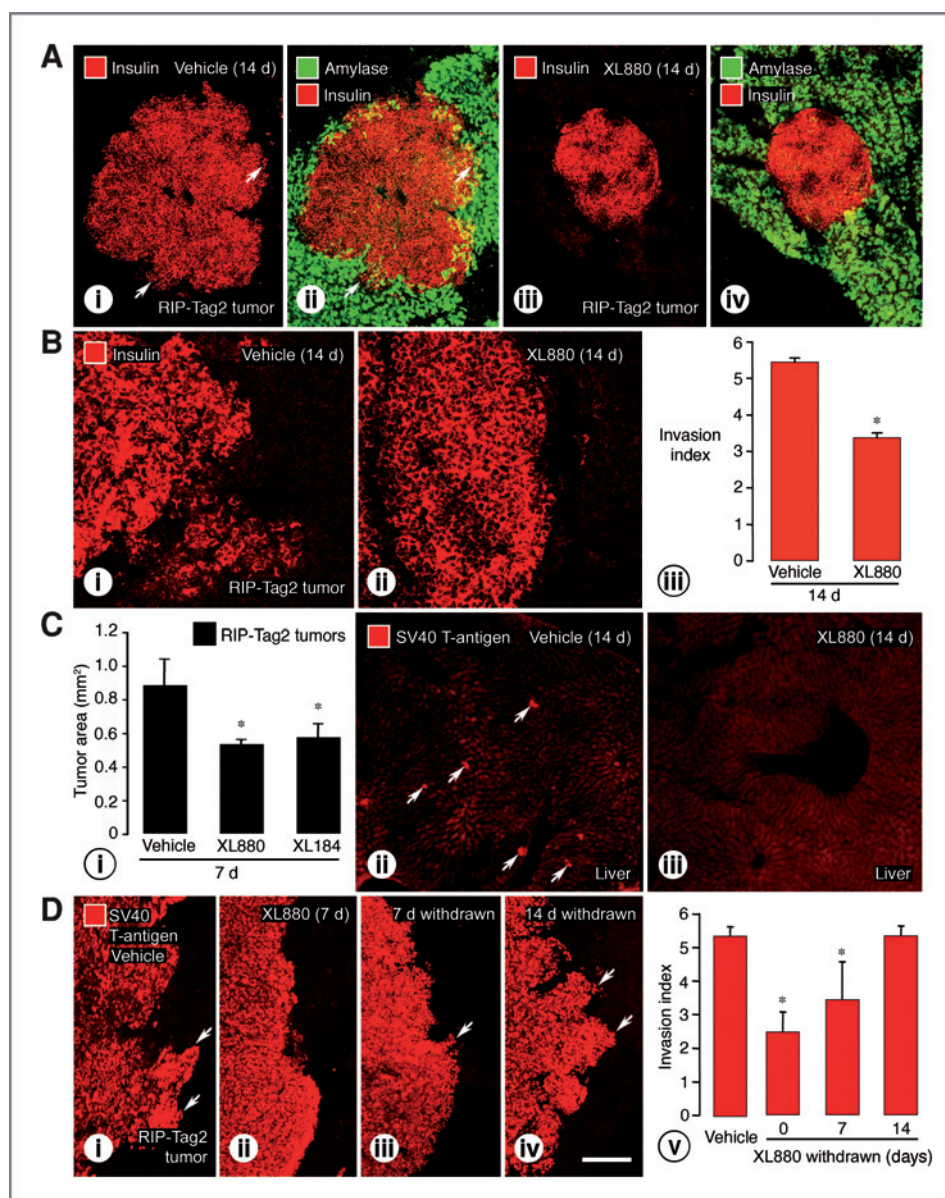


Figure 6. Treatment-related differences in tumor invasiveness, size, and liver metastases. Confocal micrographs of RIP-Tag2 tumors. A, i and ii, irregular border (arrows) of tumor after vehicle treatment. A, iii and iv, smooth contour of tumor after XL880 treatment for 14 days. Tumor cells stained for insulin (red) and surrounding exocrine pancreas stained for amylase (green). B, i–iii, measurements show significant reduction in irregularity of tumor border, reflected by Invasion index, after XL880 treatment for 14 days. C, i, measurements of histologic sections show significant reductions in size of RIP-Tag2 tumors after treatment with XL880 (40%) or XL184 (35%) for 7 days, from age 10 to 11 weeks. C, ii and iii, scattered tumor cells (arrows) marked by SV40 T-antigen immunoreactivity are shown in the liver of 12-week-old RIP-Tag2 mouse after treatment with vehicle, but no stained cells after XL880 treatment, for 14 days. D, i, irregular tumor border after vehicle (arrows). D, ii, smoother tumor border after XL880 treatment for 7 days. D, iii, smooth border with small projections at 7 days after withdrawal of XL880 (arrows). D, iv, greater irregularity of tumor border (arrows) at 14 days, which is similar to, but not more severe than, baseline. D, v, Invasion index measurements show the magnitude of changes in tumor border irregularity before and after withdrawal. *, P < 0.05 versus vehicle. Scale bar, 150 μm (A); 55 μm (B); 180 μm (C); 50 μm (D).

inhibitors (4, 36, 41), but the decrease was less. Basement membrane sleeves depend in part on the viability of the associated endothelial cells and/or pericytes, but they were not lost proportionally: endothelial cells were reduced by 80%, pericytes by 71%, and basement membrane by only 52%.

Tumor vessels rapidly regrow after withdrawal of VEGF inhibitors (36). Tumor vessels also regrew after withdrawal of XL880 or XL184, but the regrowth was slowed. Although the mechanism is uncertain, one factor for the reduced vascular regrowth after XL880 or XL184 treatment may be the greater loss of pericytes and basement membrane sleeves that provide a scaffold for regrowing blood vessels (36).

To better understand the robust effects of XL880 and XL184 on blood vessels in RIP-Tag2 tumors, we examined the amount and distribution of c-Met immunoreactivity.

Strong staining for c-Met was consistently found in some tumor vessels at baseline. Colocalization with CD31 indicated the vascular staining of c-Met was restricted to endothelial cells. In addition, some tumor cells marked by SV40 T-antigen had faint c-Met immunoreactivity. Vascular staining for c-Met was conspicuously less after XL880 or XL184 treatment but was unchanged after XL999 treatment. Consistent with this finding, total c-Met and phosphorylated c-Met, assessed by immunoprecipitation, were both reduced after XL184 treatment, but neither was significantly reduced after XL999 treatment. On the basis of intensity of c-Met immunoreactivity, vascular endothelial cells probably made a significant contribution to the signal in the immunoblots and were targets of XL880 and XL184, but the presence of weak staining in tumor cells indicates that c-Met blockade is

also likely to have direct effects on tumor cells in the RIP-Tag2 model.

The robust effects of XL880 and XL184 on RIP-Tag2 tumors were not limited to tumor vessels. Intratumoral hypoxia and tumor cell apoptosis were also widespread. Induction of hypoxia and apoptosis was probably due to the extensive and progressive pruning of tumor vessels without vessel normalization. The association of pimonidazole staining with regions of tumor that had few or no blood vessels is consistent with this interpretation.

Invasiveness, which is a typical feature of aggressive tumors (42, 43), increases in some preclinical models after inhibition of VEGF (5, 6, 44, 45). Treatment with XL880 resulted in smaller and less invasive tumors in RIP-Tag2 mice, and, importantly, recovery of tumor invasiveness was slowed and did not rebound at an exaggerated rate during the first 2 weeks after XL880 was withdrawn.

The involvement of c-Met in the anti-invasive action of XL880 and XL184 is consistent with their potent inhibitory actions on c-Met, the presence of c-Met immunoreactivity in RIP-Tag2 tumors under baseline conditions, and the reduction in c-Met and invasiveness after treatment. XL880 and XL184 had IC₅₀ values for c-Met of 0.4 and 1.3 nmol/L compared with 463 nmol/L for XL999. Involvement of c-Met also fits with the reduction in phospho-c-Met protein in the tumors after treatment with XL184. XL999 lacked the robust effect of XL880 and XL184 on apoptosis of blood vessels and tumor cells in RIP-Tag2 tumors. Although inhibition of AXL could contribute to the anti-invasive action, as reported in other models (46–49), this is unlikely to be the main target because XL880, XL184, and XL999 block AXL about equally, with IC₅₀ values in the range of 4.6 to 11 nmol/L.

The kinase profiles of XL880, XL184, and XL999 had differences in addition to c-Met, and drug efficacy is also influenced by *in vivo* absorption, stability, clearance, and other chemical properties that influence pharmacokinetics and pharmacodynamics. Therefore, confirmation of essential or exclusive roles of inhibition of c-Met and VEGFR in the anti-invasive effects of XL880 and XL184 will require the use of more selective

inhibitors, comparison of drug actions after genetic deletion of c-Met, or other strategies that target these signaling pathways without impacting other receptors.

In conclusion, we found that XL880 and XL184 caused rapid and extensive regression of endothelial cells and pericytes of blood vessels in RIP-Tag2 tumors. Regression of the tumor vasculature was widespread, progressive, and accompanied by extensive intratumoral hypoxia and apoptosis of tumor cells. The treated tumors were smaller, less invasive, and accompanied by fewer liver metastases. The findings are consistent with the distinctive antitumoral actions of XL880 and XL184 resulting from inhibition of VEGFR and c-Met together. However, inhibition of other receptors and chemical properties that influence pharmacokinetics and pharmacodynamics could also contribute. Careful assessment using strategies for selective inhibition or knockdown of individual receptors or pathways will be necessary to determine whether inhibition of VEGFR and c-Met is necessary and sufficient to reproduce all of the robust effects of XL880 and XL184 on tumors.

Disclosure of Potential Conflicts of Interest

D.T. Aftab is employed by Exelixis Inc.

Acknowledgments

The authors thank Rolf Brekken of the University of Texas Southwestern Medical Center for the VEGFR-2 antibody, Peter Baluk and Christophe Colas for valuable advice and discussions, and Jie Wei for genotyping the mice.

Grant Support

This study was supported by NIH grants HL24136 and HL59157 from the National Heart, Lung, and Blood Institute; CA82923 from the National Cancer Institute; a grant from Exelixis Inc.; and funding from AngelWorks Foundation to D.M. McDonald.

The costs of publication of this article were defrayed in part by the payment of page charges. This article must therefore be hereby marked *advertisement* in accordance with 18 U.S.C. Section 1734 solely to indicate this fact.

Received July 13, 2010; revised January 27, 2011; accepted May 17, 2011; published OnlineFirst May 25, 2011.

References

- Ferrara N, Chen H, Davis-Smyth T, Gerber HP, Nguyen TN, Peers D, et al. Vascular endothelial growth factor is essential for corpus luteum angiogenesis. *Nat Med* 1998;4:336–40.
- Brekken RA, Overholser JP, Stastny VA, Waltenberger J, Minna JD, Thorpe PE. Selective inhibition of vascular endothelial growth factor (VEGF) receptor 2 (KDR/Flik-1) activity by a monoclonal anti-VEGF antibody blocks tumor growth in mice. *Cancer Res* 2000;60:5117–24.
- Jain RK. Normalizing tumor vasculature with anti-angiogenic therapy: a new paradigm for combination therapy. *Nat Med* 2001;7:987–9.
- Inai T, Mancuso M, Hashizume H, Baffert F, Haskell A, Baluk P, et al. Inhibition of vascular endothelial growth factor (VEGF) signaling in cancer causes loss of endothelial fenestrations, regression of tumor vessels, and appearance of basement membrane ghosts. *Am J Pathol* 2004;165:35–52.
- Paez-Ribes M, Allen E, Hudock J, Takeda T, Okuyama H, Viñals F, et al. Antiangiogenic therapy elicits malignant progression of tumors to increased local invasion and distant metastasis. *Cancer Cell* 2009;15:220–31.
- Ebos JM, Lee CR, Cruz-Munoz W, Bjarnason GA, Christensen JG, Kerbel RS. Accelerated metastasis after short-term treatment with a potent inhibitor of tumor angiogenesis. *Cancer Cell* 2009;15:232–9.
- Hayden EC. Cutting off cancer's supply lines. *Nature* 2009;458:686–7.
- Loges S, Mazzone M, Hohnsinner P, Carmeliet P. Silencing or fueling metastasis with VEGF inhibitors: antiangiogenesis revisited. *Cancer Cell* 2009;15:167–70.
- Goodman VL, Rock EP, Dagher R, Ramchandani RP, Abraham S, Gobburu JV, et al. Approval summary: sunitinib for the treatment of imatinib refractory or intolerant gastrointestinal stromal tumors and advanced renal cell carcinoma. *Clin Cancer Res* 2007;13:1367–73.
- Rock EP, Goodman V, Jiang JX, Mahjoob K, Verbois SL, Morse D, et al. Food and Drug Administration drug approval summary: sunitinib malate for the treatment of gastrointestinal stromal tumor and advanced renal cell carcinoma. *Oncologist* 2007;12:107–13.
- Cohen MH, Gootenberg J, Keegan P, Pazdur R. FDA drug approval summary: bevacizumab (Avastin) plus carboplatin and paclitaxel as first-line treatment of advanced/metastatic recurrent nonsquamous non-small cell lung cancer. *Oncologist* 2007;12:713–8.

12. Bergers G, Hanahan D. Modes of resistance to anti-angiogenic therapy. *Nat Rev Cancer* 2008;8:592–603.
13. Ferrara N, Kerbel RS. Angiogenesis as a therapeutic target. *Nature* 2005;438:967–74.
14. de Jonge MJ, Verweij J. Multiple targeted tyrosine kinase inhibition in the clinic: all for one or one for all? *Eur J Cancer* 2006;42:1351–6.
15. Bussolino F, Di Renzo MF, Ziche M, Bocchietto E, Olivero M, Naldini L, et al. Hepatocyte growth factor is a potent angiogenic factor which stimulates endothelial cell motility and growth. *J Cell Biol* 1992;119:629–41.
16. Benvenuti S, Comoglio PM. The MET receptor tyrosine kinase in invasion and metastasis. *J Cell Physiol* 2007;213:316–25.
17. Christensen J, Anders K. Beyond VEGF: targeting tumor growth and angiogenesis via alternative mechanisms. *Adv Exp Med Biol* 2008;610:43–53.
18. Cecchi F, Rabe DC, Bottaro DP. Targeting the HGF/Met signalling pathway in cancer. *Eur J Cancer* 2010;46:1260–70.
19. To CT, Tsao MS. The roles of hepatocyte growth factor/scatterfactor and Met receptor in human cancers [review]. *Oncol Rep* 1998;5:1013–24.
20. Birchmeier C, Birchmeier W, Gherardi E, Vande Woude GF. Met, metastasis, motility and more. *Nat Rev Mol Cell Biol* 2003;4:915–25.
21. Kuba K, Matsumoto K, Date K, Shimura H, Tanaka M, Nakamura T. HGF/NK4, a four-kringle antagonist of hepatocyte growth factor, is an angiogenesis inhibitor that suppresses tumor growth and metastasis in mice. *Cancer Res* 2000;60:6737–43.
22. Christensen JG, Schreck R, Burrows J, Kuruganti P, Chan E, Le P, et al. A selective small molecule inhibitor of c-Met kinase inhibits c-Met-dependent phenotypes *in vitro* and exhibits cytoreductive anti-tumor activity *in vivo*. *Cancer Res* 2003;63:7345–55.
23. Michieli P, Mazzone M, Basilico C, Cavassa S, Sottile A, Naldini L, et al. Targeting the tumor and its microenvironment by a dual-function decoy Met receptor. *Cancer Cell* 2004;6:61–73.
24. Martens T, Schmidt NO, Eckerich C, Fillbrandt R, Merchant M, Schwall R, et al. A novel one-armed anti-c-Met antibody inhibits glioblastoma growth *in vivo*. *Clin Cancer Res* 2006;12:6144–52.
25. Pennacchietti S, Michieli P, Galluzzo M, Mazzone M, Giordano S, Comoglio PM. Hypoxia promotes invasive growth by transcriptional activation of the met protooncogene. *Cancer Cell* 2003;3:347–61.
26. Bottaro DP, Liotta LA. Cancer: out of air is not out of action. *Nature* 2003;423:593–5.
27. Qian F, Engst S, Yamaguchi K, Yu P, Won KA, Mock L, et al. Inhibition of tumor cell growth, invasion, and metastasis by EXEL-2880 (XL880, GSK1363089), a novel inhibitor of HGF and VEGF receptor tyrosine kinases. *Cancer Res* 2009;69:8009–16.
28. Salgia R, Hong DS, Camacho LH,, Ng CS, Janisch L, Ratain MJ, et al. A phase I dose-escalation study of the safety and pharmacokinetics (PK) of XL184, a VEGFR and MET kinase inhibitor, administered orally to patients (pts) with advanced malignancies. *J Clin Oncol* 2007;25:14031.
29. Salgia R, Sherman S, Hong DS,, Ng CS, Frye J, Janisch L, et al. A phase I study of XL184, a RET, VEGFR2, and MET kinase inhibitor, in patients (pts) with advanced malignancies, including pts with medullary thyroid cancer (MTC). *J Clin Oncol* 2008;26:3522.
30. Bean J, Brennan C, Shih JY, Riely G, Viale A, Wang L, et al. MET amplification occurs with or without T790M mutations in EGFR mutant lung tumors with acquired resistance to gefitinib or erlotinib. *Proc Natl Acad Sci U S A* 2007;104:20932–7.
31. Liu L, Greger J, Shi H, Liu Y, Greshock J, Annan R, et al. Novel mechanism of lapatinib resistance in HER2-positive breast tumor cells: activation of AXL. *Cancer Res* 2009;69:6871–8.
32. Joly AH. Simultaneous blockade of VEGF and HGF receptors results in potent anti-angiogenic and anti-tumor effects. *Eur J Cancer* 2006; Suppl 4:35. Abstract nr 104.
33. Cripe L, McGuire W, Wertheim M, Eisenberg P, Stadler W, Paquette R, et al. Integrated report of the phase 2 experience with XL999 administered IV to patients (pts) with NSCLC, renal cell CA (RCC), metastatic colorectal CA (CRC), recurrent ovarian CA, acute myelogenous leukemia (AML), and multiple myeloma (MM). *J Clin Oncol* 2007;25:3591.
34. Aftab D. The spectrum-selective kinase inhibitor EXEL-0999 inhibits mitogenic and angiogenic kinases, and causes rapid tumor vasculature destruction and regression in mouse xenograft models. *Eur J Cancer* 2004;Suppl 2:141.
35. Hanahan D. Heritable formation of pancreatic beta-cell tumors in transgenic mice expressing recombinant insulin/simian virus 40 oncogenes. *Nature* 1985;315:115–22.
36. Mancuso MR, Davis R, Norberg SM, O'Brien S, Sennino B, Nakahara T, et al. Rapid vascular regrowth in tumors after reversal of VEGF inhibition. *J Clin Invest* 2006;116:2610–21.
37. Baffert F, Thurston G, Rochon-Duck M, Le T, Brekken R, McDonald DM. Age-related changes in vascular endothelial growth factor dependency and angiopoietin-1-induced plasticity of adult blood vessels. *Circ Res* 2004;94:984–92.
38. Baffert F, Le T, Sennino B, Thurston G, Kuo CJ, Hu-Lowe D, et al. Cellular changes in normal blood capillaries undergoing regression after inhibition of VEGF signaling. *Am J Physiol Heart Circ Physiol* 2006;290:H547–59.
39. Kamba T, Tam BY, Hashizume H, Haskell A, Sennino B, Mancuso MR, et al. VEGF-dependent plasticity of fenestrated capillaries in the normal adult microvasculature. *Am J Physiol Heart Circ Physiol* 2006;290:H560–76.
40. von Burstin J, Eser S, Paul MC, Seidler B, Brandl M, Messer M, et al. E-cadherin regulates metastasis of pancreatic cancer *in vivo* and is suppressed by a SNAI1/HDAC1/HDAC2 repressor complex. *Gastroenterology* 2009;137:361–71.
41. Nakahara T, Norberg SM, Shalinsky DR, Hu-Lowe DD, McDonald DM. Effect of inhibition of vascular endothelial growth factor signaling on distribution of extravasated antibodies in tumors. *Cancer Res* 2006;66:1434–45.
42. Bergers G, Brekken R, McMahon G, Vu TH, Itoh T, Tamaki K, et al. Matrix metalloproteinase-9 triggers the angiogenic switch during carcinogenesis. *Nat Cell Biol* 2000;2:737–44.
43. Joyce JA, Baruch A, Chehade K, Meyer-Morse N, Giraudo E, Tsai FY, et al. Cathepsin cysteine proteases are effectors of invasive growth and angiogenesis during multistage tumorigenesis. *Cancer Cell* 2004;5:443–53.
44. Casanovas O, Hicklin DJ, Bergers G, Hanahan D. Drug resistance by evasion of antiangiogenic targeting of VEGF signaling in late-stage pancreatic islet tumors. *Cancer Cell* 2005;8:299–309.
45. Du R, Lu KV, Petritsch C, Liu P, Ganss R, Passegue E, et al. HIF1alpha induces the recruitment of bone marrow-derived vascular modulatory cells to regulate tumor angiogenesis and invasion. *Cancer Cell* 2008;13:206–20.
46. Li Y, Ye X, Tan C, Hongo JA, Zha J, Liu J, et al. Axl as a potential therapeutic target in cancer: role of Axl in tumor growth, metastasis and angiogenesis. *Oncogene* 2009;28:3442–55.
47. Holland SJ, Pan A, Franci C, Hu Y, Chang B, Li W, et al. R428, a selective small molecule inhibitor of Axl kinase, blocks tumor spread and prolongs survival in models of metastatic breast cancer. *Cancer Res* 2010;70:1544–54.
48. Ye X, Li Y, Stawicki S, Couto S, Eastham-Anderson J, Kallop D, et al. An anti-Axl monoclonal antibody attenuates xenograft tumor growth and enhances the effect of multiple anticancer therapies. *Oncogene* 2010;29:5254–64.
49. Gjerdrum C, Tiron C, Høiby T, Stefansson I, Haugen H, Sandal T, et al. Axl is an essential epithelial-to-mesenchymal transition-induced regulator of breast cancer metastasis and patient survival. *Proc Natl Acad Sci U S A* 2010;107:1124–9.
50. Wilhelm S, Carter C, Lynch M, Lowinger T, Dumas J, Smith RA, et al. Discovery and development of sorafenib: a multikinase inhibitor for treating cancer. *Nat Rev Drug Discov* 2006;5:835–44.